Ocean Sci. Discuss., 8, 1–28, 2011
www.ocean-sci-discuss.net/8/1/2011/
doi:10.5194/osd-8-1-2011

Ocean Science Discussions

High frequency variability of the Atlantic meridional overturning circulation

B. Balan Sarojini[1,2], J. M. Gregory[1,2,3], R. Tailleux[2], G. R. Bigg[4], A. T. Blaker[5], D. Cameron[6], N. R. Edwards[7], A. P. Megann[5], L. C. Shaffrey[1,2], and B. Sinha[5]

[1]National Centre for Atmospheric Science – Climate Division, Reading, UK
[2]Walker Institute, University of Reading, Reading, UK
[3]Met Office Hadley Centre, Exeter, UK
[4]Department of Geography, University of Sheffield, Sheffield, UK
[5]National Oceanography Centre, Southampton, UK
[6]Centre for Ecology and Hydrology, Edinburgh, UK
[7]Earth and Environmental Sciences, The Open University, Milton Keynes, UK

Received: 19 November 2010 – Accepted: 14 January 2011 – Published:

Correspondence to: B. Balan Sarojini (b.balansarojini@reading.ac.uk)

Published by Copernicus Publications on behalf of the European Geosciences Union.

Abstract

We compare the variability of the Atlantic meridional overturning circulation (AMOC) as simulated by the coupled climate models of the RAPID project, which cover a wide range of resolution and complexity, and observed by the RAPID/MOCHA array at about 26° N. We analyse variability on a range of timescales. In models of all resolutions there is substantial variability on timescales of a few days; in most AOGCMs the amplitude of the variability is of somewhat larger magnitude than that observed by the RAPID array, while the amplitude of the simulated annual cycle is similar to observations. A dynamical decomposition shows that in the models, as in observations, the AMOC is predominantly geostrophic (driven by pressure and sea-level gradients), with both geostrophic and Ekman contributions to variability, the latter being exaggerated and the former underrepresented in models. Other ageostrophic terms, neglected in the observational estimate, are small but not negligible. In many RAPID models and in models of the Coupled Model Intercomparison Project Phase 3 (CMIP3), interannual variability of the maximum of the AMOC wherever it lies, which is a commonly used model index, is similar to interannual variability in the AMOC at 26° N. Annual volume and heat transport timeseries at the same latitude are well-correlated within 15–45° N, indicating the climatic importance of the AMOC. In the RAPID and CMIP3 models, we show that the AMOC is correlated over considerable distances in latitude, but not the whole extent of the North Atlantic; consequently interannual variability of the AMOC at 50° N is not well-correlated with the AMOC at 26° N.

1 Introduction

Any substantial change, whether anthropogenic or natural, in the meridional overturning circulation of the Atlantic Ocean (AMOC) could considerably affect the climate, especially of the North Atlantic and Europe, on account of the associated northward ocean heat transport. A complete cessation of the AMOC would produce a strong

OSD
8, 1–28, 2011

cooling (Vellinga and Wood, 2002; Stouffer et al., 2006), but this is very unlikely during the 21st century according to the latest assessment of the Intergovernmental Panel on Climate Change (Meehl et al., 2007). Schmittner et al. (2005) and Meehl et al. (2007) show that there exists a wide range of weakening – from 0% to 50% – of the AMOC by 2100 in model projections of climate change under scenarios of increasing anthropogenic greenhouse gas concentrations. Other studies (Knight et al., 2005; Keenlyside et al., 2008) suggest that AMOC may weaken over the next decade due to unforced (natural) variability, resulting in a cooler climate around the North Atlantic. The internally generated interannual variability of the AMOC in coupled AOGCMs (Dong and Sutton, 2001; Collins et al., 2006) and in ocean-alone GCMs (Biastoch et al., 2008) is found to be closely linked to interannual variations in Atlantic Ocean heat transport (AOHT). Understanding the unforced interannual variability of the AMOC and AOHT is important because it is the background against which any signal of climate change has to be detected.

Because of such considerations, the RAPID/MOCHA array (Cunningham et al., 2007) was deployed at 26.5° N in the Atlantic Ocean to monitor the AMOC and provide information about its variability. The array data show temporal variability in the AMOC on a range of time scales, including time scales of a few days. This part of the AMOC variability spectrum has not been much studied in the numerical models used for climate projections. The question thus arises of whether they are able to represent it realistically.

The high-frequency AMOC variability simulated by two climate models is assessed in Baehr et al. (2009) using the first year of data from the RAPID array. They found that the magnitude of variability is well reproduced in ECHAM5/MPI-OM, and ECCO-GODAE shows significant correlation of the daily AMOC to that of the RAPID/MOCHA time series. The ECCO-GODAE time series is expected to correlate to that of RAPID array because the model is forced by NCEP/NCAR reanalysis fluxes for the one-year analysis period and prior to that the model solution is evolved using an optimised initial state from many observational datasets. Comparison with other models is valuable to assess

OSD
8, 1–28, 2011

model systematic uncertainty and study its causes (e.g., Gregory et al., 2005; Stouffer et al., 2006). The RAPID programme, which established the observational array, also includes an intercomparison project of UK global climate models (the RAPID-models) of varying resolution and complexity. The work presented here aims to answer the following questions: (a) whether the RAPID-models simulate high-frequency variability in the AMOC, (b) how they compare to the 5-year long RAPID/MOCHA observational estimates and (c) whether the volume transport and heat transport at different timescales and at various latitudes in the North Atlantic are related.

2 Data – models and measurements

The RAPID-models, namely HadCM3, FAMOUS, FORTE, FRUGAL, GENIE, CHIME and HiGEM, are all global coupled atmosphere ocean models without flux adjustments. They are all employed for investigations of climate variability and change on various timescales. The specifications of their atmosphere and ocean components are summarised in Table 1.

HadCM3 (Gordon et al., 2000) is a Hadley Centre atmosphere–ocean general circulation model (AOGCM) which has been used successfully for many purposes and extensively cited, for instance in the IPCC Fourth Assessment Report. FAMOUS (Jones et al., 2005; Smith et al., 2008) is a low-resolution version of HadCM3, calibrated to replicate HadCM3 climate as closely as possible. It runs ten times faster than HadCM3, making it a computationally less expensive AOGCM for long-term or large ensembles of climate simulations. HiGEM (Shaffrey et al., 2009) is a high-resolution AOGCM derived originally from the Hadley Centre AOGCM HadGEM1. Compared to HadCM3, the predecessor of HadGEM1, HiGEM has new atmospheric and sea-ice dynamics submodels together with substantial differences such as a linear-free surface, a 4th order advection scheme, 40 vertical levels and the Gent-McWilliams mixing scheme being turned off. It has an eddy-permitting ocean and allows fine spatial and temporal coupling between the ocean and atmosphere. HiGEM is intended for decadal climate

OSD
8, 1–28, 2011

prediction; it is computationally expensive but several multi-decadal runs with it have been completed. FORTE (Blaker et al., 2010) uses a recoded version (MOMA, Webb, 1996) of the Modular Ocean Model (MOM) (Pacanowski, 1990). It is similar to that of the Hadley Centre models and is at a resolution between the HadCM3 and FAMOUS ocean, but has a spectral atmospheric dynamics submodel with higher resolution than the HadCM3 atmosphere and simpler atmospheric physics. CHIME (Megann et al., 2010) couples the atmosphere model of HadCM3 with a predominantly isopycnic ocean (hybrid-coordinate ocean, HYCOM, Bleck, 2002), the only RAPID-model using such a scheme rather than horizontal levels of fixed depth, permitting an investigation of the consequences of this aspect of model formulation. FRUGAL (Bigg and Wadley, 2001) has an energy-moisture balance advective-diffusive atmospheric component, based on the UVic model of Weaver et al. (2001). It does not simulate winds, and a prescribed wind-stress climatology is applied to the ocean. FRUGAL uses the MOM ocean with a grid designed to improve resolution of the Arctic Ocean. GENIE (Edwards and Marsh, 2005) also uses the UVic atmosphere and is the only RAPID-model which does not have a primitive-equation ocean model; instead, it uses a frictional geostrophic model (GOLDSTEIN) in which horizontal momentum diffusion is parameterised by Rayleigh friction rather than viscosity. This is computationally very cheap and consequently GENIE is the fastest RAPID-model by a large factor, suiting its intended use for multimillennial climate simulations and very large ensembles.

For this analysis, we produced 10 years of 5-daily model data (i.e. 5-day means) from the unforced control integrations of the models. For calculation of the interannual variability of the model AMOC, we also produced time-series of 110 years of annual means from the control integrations. The data analysed in this paper comes from portions of the control runs after the models have been spun up for many hundred years except in HiGEM and CHIME where the control runs are only 115 and 200 years long, respectively. The 5-daily data in CHIME and HiGEM is from year 60 to year 70 and the annual data in CHIME is from year 60 to year 170. In HiGEM, the annual data is only 90 years long, after the spin-up time.

OSD
8, 1–28, 2011

The RAPID/MOCHA array is the first of its kind to monitor the basin-wide transport at a latitude. It is designed to estimate the AMOC as the sum of three observable components namely, Ekman transport, Florida Current transport and the upper mid-ocean transports (see Sect. 4 for more details). Note that it is an observational estimate of a composite of the main contributions with an unknown residual term that is assumed to be small and barotropic. It does not include other ageostrophic components than the Ekman component. The array has temporally high sampling, i.e. 12-hourly but does not have spatially high sampling across the latitude and depths. The observational timeseries are 5 years long, from April 2004 to March 2009. We average the 12-hourly measurements (10-day low-pass filtered) to produce 5-daily data for comparison to the 5-daily model data. The 5-daily data has a standard deviation only 3.2% less than that of the 12-hourly data.

3 Comparison of simulated and observed variability

We calculate the timeseries of the 5-daily Atlantic meridional overturning transport at about 26° N in models and measurements. The overturning transport T_{over} at a given latitude y and time t is the zonal and vertical integral of the meridional velocity v

$$T_{\text{over}}(y,t) = \int_z^0 \int v(x,y,z',t)\,dx\,dz' \tag{1}$$

where x and z are the zonal and vertical axes respectively and the zonal integral is across the whole width of the Atlantic Basin. We take the depth integral from the surface ($z = 0$) to a depth of 1000 m approximately, to include all of the northward branch of the AMOC. The precise latitude and depth for evaluating T_{over} are chosen for each model to coincide with a boundary between model cells in each direction and are shown in Table 1. By construction, the value of T_{over} is identical with the meridional overturning streamfunction at the given latitude and depth. At about 26° N, all models have a long-term mean strength in the range 16–21 Sv, comparable with 18.6 Sv observed

OSD
8, 1–28, 2011

(Table 1). HiGEM has the smallest time-mean and FAMOUS the largest. The T_{over} in HiGEM has a lower time-mean compared to that in Shaffrey et al. (2009) because of a difference in the two definitions of T_{over}. Their definition is the maximum value of the overturning streamfunction at 26° N whereas ours is the integral of the northward velocity above about 1000 m.

Substantial variability on short time scales is evident in models as well as in observations in the timeseries for a single year (Fig. 1a), shown as an illustration. Calculating the 5-daily standard deviation at 26° N for this single year gives 3–4 Sv for the observations and all the models except FRUGAL and GENIE (Table 1). This is remarkable, given the wide range of complexity of the models, and it is interesting that the magnitude of simulated variability does not depend on model resolution. GENIE and FRUGAL have no high-frequency variability. These models use the UVic atmosphere model, which does not have internal dynamics capable of generating variability. It is likely that in the other models the atmosphere provides most of the ocean variability (Gregory et al., 2005).

A single year is not representative of climatological statistics, so we calculate the mean annual cycle from the 10 individual years for each model and the 5 years of observations (Fig. 1b). The high-frequency variability is thereby reduced, but still notable; the 5-daily standard deviation remains similar across most models and is slightly larger in observations (Table 1). Part of the variability comes from the annual cycle. The observations show a maximum in autumn and a minimum in spring whereas the models show a range of seasonal behaviour.

The variance spectra of the time series (Fig. 1c) show that the annual cycle is the dominant period in both models and observations. In all the models, its variance is within a factor of two of that of observations. At the highest frequencies, however, all the models except CHIME have greater variance than observations, by up to an order of magnitude; interestingly, there is no systematic dependence on model resolution. FAMOUS shows particularly large variance in shorter periods. CHIME shows least variance both for the annual cycle and at high frequencies. Since it uses the same

OSD
8, 1–28, 2011

atmosphere model as HadCM3, this difference must be due to the ocean model in some way. Oscillations of less than 40-day period are significant in all the models (except FRUGAL and GENIE) and observations.

In Fig. 1d we show the annual timeseries of T_{over} at 26° N. The observed timeseries is not yet long enough to assess variability on multiannual timescales. FAMOUS and CHIME have greater long-period variability than other models.

4 Dynamical decomposition of the transport

In order to identify the physical sources of variability in the simulated overturning, a dynamical decomposition of the transport is carried out on the 5-daily timeseries. Previous modelling studies (Hirschi et al., 2003; Baehr et al., 2009) suggest various ways of doing this. Cunningham et al. (2007) decompose the observational T_{over} from the RAPID/MOCHA array into Ekman, Florida Current and upper mid-ocean components. The Ekman component is physically distinguished; it exists within the upper tens of metres which are affected by the windstress and the vertical shear it causes. The Florida Current component is geographically distinguished; it is the integral of flow at all depths passing through the narrow channel between Florida and the Bahamas, within which there is a specific monitoring system. The channel is 800 m deep and the flow through it is entirely counted in the northward branch of the AMOC. The upper mid-ocean component is the geostrophic meridional flow above 1100 m through the 26.5° N section across the Atlantic from the Bahamas to Africa.

Florida and the Bahamas are not represented with realistic geography, or at all, in the models. Hence we cannot meaningfully calculate the Florida Straits current, and instead we carry out the decomposition slightly further north, at around 29° N, between the coasts of America and Africa. Again, the precise latitude is model-dependent, and the same depth is used as for 26° N (Table 1). Our decomposition of T_{over} is physically based, consistent with the model formulations, into Ekman, geostrophic, viscous and advective components.

OSD
8, 1–28, 2011

Consider the equation of motion. The zonal acceleration is given as

$$\frac{Du}{Dt} = \boldsymbol{u}\cdot\nabla u + \frac{\partial u}{\partial t} = -\frac{1}{\rho}\frac{\partial P}{\partial x} + fv + F_v + F_h \tag{2}$$

where $\boldsymbol{u}$ is the 3-D velocity and u its eastward component, $\partial P/\partial x$ is the zonal pressure gradient, f is the Coriolis parameter, $F_v = \kappa\partial^2 u/\partial z^2$ is the vertical momentum diffusion term with κ the coefficient of vertical viscosity, $F_h = \eta\nabla_H^2 u$ and/or $\eta\nabla_H^4 u$ (according to model formulation) is the horizontal momentum diffusion term with η being the coefficient of horizontal viscosity, and ρ is the Boussinesq reference density. We rearrange Eq. (2) and integrate it over depth and longitude across the Atlantic as

$$\int_z^0 \int v\,dx\,dz' = \frac{1}{f}\int_z^0 \int \left(\frac{1}{\rho}\frac{\partial P}{\partial x} - F_v - F_h + \boldsymbol{u}\cdot\nabla u + \frac{\partial u}{\partial t}\right) dx\,dz' \tag{3}$$

Thus we treat the total transport on the LHS as a sum of the terms on the RHS as follows.

The geostrophic transport (T_{geo}) is the term due to $\partial P/\partial x$ and consists of two parts: the internal part (T_{int}), which is due to the pressure gradient $\partial P_\rho/\partial x$ caused by zonal density gradients, and the external part (T_{ext}), which is due to the sea surface slope $\partial h/\partial x$ in models with a free surface (HiGEM, FORTE) or to the rigid lid pressure gradient $\partial P_s/\partial x$ in rigid lid models (HadCM3, FAMOUS and GENIE), where effectively $P_s = h\rho g$. Thus

$$T_{\text{geo}} = T_{\text{ext}} + T_{\text{int}}, \qquad T_{\text{int}} = \frac{1}{\rho f}\int_z^0 \int \frac{\partial P_\rho}{\partial x}\,dx\,dz', \qquad T_{\text{ext}} = \frac{1}{\rho f}\int_z^0 \int \frac{\partial P_s}{\partial x}\,dx\,dz' \tag{4}$$

The vertical momentum diffusion $\kappa\partial^2 u/\partial z^2$ is the vertical derivative of the diffusive vertical momentum flux $\kappa\partial u/\partial z$. Integrated over the upper ocean, this equals the surface momentum flux i.e. the zonal wind stress τ_x, which is all absorbed in the Ekman layer. The bottom boundary layer is far below, and the bottom stress is identically zero in

OSD
8, 1–28, 2011

HadCM3 and FAMOUS, which have a free-slip bottom boundary condition, and is negligible in HiGEM and FORTE. GENIE has no bottom boundary layer or explicit bottom stress. Hence there is no contribution from bottom stress to the Ekman transport

$$T_{\mathrm{Ek}} = -\frac{1}{\rho f}\int \tau_x \, dx. \tag{5}$$

The ageostrophic transport due to the horizontal momentum diffusion i.e. horizontal viscosity is

$$T_{\mathrm{vis}} = -\frac{1}{f}\int_z^0 \int \eta \nabla_{\mathrm{H}}^2 u \, dx \, dz' \quad \text{or} \quad T_{\mathrm{vis}} = -\frac{1}{f}\int_z^0 \int \eta \nabla_{\mathrm{H}}^4 u \, dx \, dz' \tag{6}$$

The horizontal diffusion terms are Laplacian ($\nabla_{\mathrm{H}}^2 u$) and/or biharmonic ($\nabla_{\mathrm{H}}^4 u$) formulations with different coefficient of viscosity in each model. In theory these viscous terms represent the horizontal momentum flux due to unresolved eddies, although in practice horizontal viscosity is increased to ensure model dynamical stability. The viscous term can locally be of either sign, since its effect is to transport momentum. Globally, it must sum to zero for momentum, but is a positive definite sink of kinetic energy.

The advective transport (T_{adv}) due to the non-linear advective term $\boldsymbol{u}\cdot\boldsymbol{\nabla} u$ is

$$T_{\mathrm{adv}} = \frac{1}{f}\int_z^0 \int \boldsymbol{u}\cdot\boldsymbol{\nabla} u \, dx \, dz' \tag{7}$$

where the momentum flux due to resolved eddies would appear. This term is absent in GENIE by construction and found to be negligible in HadCM3, FAMOUS and FORTE. In eddy-permitting HiGEM, T_{adv} has a considerable contribution which is about 2% of the total mean transport and 17% of the total transport variability.

In HadCM3, FAMOUS and HiGEM we can calculate all the components. Any residual is due to acceleration $\partial u/\partial t$. This is not exactly zero but very small, so we ignore it in all models, so

$$T_{\mathrm{over}} = T_{\mathrm{geo}} + T_{\mathrm{Ek}} + T_{\mathrm{vis}} + T_{\mathrm{adv}} \tag{8}$$

OSD
8, 1–28, 2011

As an example, this decomposition is shown for HadCM3 in Fig. 2. In GENIE, we calculate T_{over}, T_{Ek} and T_{vis}, and infer T_{geo} as a residual. This model uses an annual climatology of windstress as a constant term, so T_{Ek} does not contribute to variability. In FORTE, we calculate T_{over}, T_{Ek} and T_{vis} due to the Laplacian diffusion term, and infer T_{geo} as the residual. This means that the biharmonic diffusion term is included in T_{geo}. This term is implicit in the model (Webb et al., 1998) and could not be calculated offline. It is relatively large and it is unclear how to interpret it physically. The components of transport could not be computed for FRUGAL and CHIME.

The mean and 5-day variability of the components of observed and simulated transports are shown in Table 1. In the mean, the geostrophic term is largest in all cases. The Ekman term is relatively small and positive, and the viscous term even smaller and negative, except in GENIE, in which the viscous (actually frictional) term is larger than in other models and the signs of these two terms are the other way round. As discussed above, the largest part of the variability is the mean annual cycle. The two main sources of this variability are T_{geo} and T_{Ek} in the models, as in observations (Cunningham et al., 2007). However, T_{geo} variability is smaller than T_{Ek} variability in models whereas in observations the reverse is true (Table 1). It is evident in Fig. 2 that the Ekman term dominates the annual cycle in HadCM3, for example. We find that T_{geo} variability tends to be underestimated in models as compared to observations. This suggests that models underestimate pressure anomalies along the eastern/western boundaries, possibly as the result of underestimating the adiabatic upwelling/downwelling processes driven by alongshore wind-stress due to the coarse resolution which spreads the effect over one grid box instead of a more confined area in reality.

As in the observed variability (Cunningham et al., 2007), the external T_{ext} and internal T_{int} components of T_{geo} in the upper 1000 m strongly anticorrelate in most models (Table 1) since by construction, $T_{geo}(z,t) = T_{int}(z,t) + T_{ext}(z,t)$, where z is a suitably chosen depth, so that $dT_{int}/dt = -dT_{ext}/dt + dT_{geo}/dt$. Indeed, this expression shows that a strong anticorrelation between T_{int} and T_{ext} should be observed whenever the fluctuations in T_{geo} become small relative to that of T_{ext} and T_{int}, mathematically when

OSD
8, 1–28, 2011

$|dT_{geo}/dt| \ll |dT_{int}/dt|$. The physical mechanism for the latter still requires further work to be fully elucidated.

Variability due to the viscous term T_{vis} is small but not quite negligible. This term is not calculated for the observational array, because it represents the effect of unresolved motion and, by definition, any quantity measured by the array has been "resolved" by it. The analogue of this term would be any contribution to T_{over} from ageostrophic motion; the observational estimate assumes that the motion is geostrophic or Ekman, as it has to do because the current is not directly measured at all, except in the Florida Straits and near the western boundary.

5 Meridional coherence of transport and its components

On the assumption that the temporal variability of the circulation is coherent throughout the basin, a commonly used AMOC index from AOGCM results is M_{max}, the maximum of the overturning streamfunction, wherever it occurs, within a range of latitude and depth in the Atlantic, rather than at fixed latitude and depth. The RAPID/MOCHA array is intended to monitor the AMOC, by measuring the circulation at only one latitude. In the model results we can investigate how well M_{max} and T_{over} at 26° N represent T_{over} at other latitudes. GENIE is omitted from this analysis because it has no high-frequency or interannual variability, and CHIME and FRUGAL because all required timeseries are not available.

Calculated from 5-day means in the RAPID-models, the time-mean M_{max} is larger than the transport at 26° N, as it must be by construction, but the variability of M_{max} is generally less (Table 1). In annual means, however, the two timeseries have similar standard deviations. We have evaluated the same statistics from the AOGCMs of the Coupled Model Intercomparison Project Phase 3 (CMIP3), finding that in 16 out of 20 of them the annual standard deviation is similar in M_{max} and at 26° N (Table 2) ("similar" when the difference between 2 standard deviations is less than 0.5 Sv); the exceptions are GISS-ER, GISS-AOM, INM-CM3.0 and IAP-FGOALS1.0g. That suggests greater

OSD
8, 1–28, 2011

coherence across latitudes at longer time periods. However, only ten of the CMIP3 models and three of the RAPID-models have high correlation (exceeding 0.5) between the two timeseries. This is likely to be because there is a time lag between 26° N and the latitudes of M_{max}. Figure 3a shows the annual standard deviation of total transport as a function of latitude. No model has a well-defined maximum, but there is generally more variability in the tropics, diminishing towards higher latitudes.

Next, we calculate the temporal correlation between different latitudes of timeseries of annual and 5-daily volume transports and their Ekman and geostrophic components, in HadCM3, FAMOUS, FORTE and HiGEM. Positive correlations are found between neighbouring latitudes in all timeseries, diminishing with increasing separation (eg., for annual timeseries in HiGEM, Fig. 4). Anticorrelation is found for widely spaced latitudes in the Ekman component. Since this component is wind-forced, the anticorrelation must indicate opposing signs of zonal windstress, occurring on opposite sides of the anomalies in atmospheric pressure and circulation that produce the windstress anomalies. It is notable that the anticorrelation is found for both 5-daily (figure not shown) and annual data, even more pronounced in the former.

We define the "correlation length" as a function of latitude y to be the width of the range of latitudes whose timeseries which have a temporal correlation exceeding 0.5 with the timeseries at latitude y. Within 15–60° N, the correlation lengths are typically 20–40° in the annual timeseries (see Table 1 for 26° N and Fig. 4 for HiGEM). Correlation lengths are greater for the annual total and the geostrophic components than for the Ekman. They are also greater for annual total transports than for 5-daily total transports, due to the greater coherence of the annual geostrophic component. Bingham et al. (2007, their Fig. 2c) also showed long-range coherence of annual total transport for HadCM3.

Given the typical correlation length, we conclude that the transport measured by the RAPID/MOCHA array is likely to have a correlation of less than 0.5 with the AMOC strength in the mid-to-high latitude Atlantic, where it has its greatest importance to climate variability (see Sect. 6). In the CMIP3 data, we test this by correlating timeseries

OSD
8, 1–28, 2011

of T_{over} at 26° N and 50° N; only two models have a coefficient exceeding 0.5. Correlation is increased somewhat by including lags of a few years, but still does not exceed 0.5 in most cases. In models where there is a lag, variability of T_{over} at 50° N precedes 26° N, indicating that the forcing of the large-scale geostrophic variability comes from the north. A similar relation between AMOC at 26° N and 50° N with a time lag of 4 years is found in GFDL-CM2.1 (Zhang, 2010).

6 Relation of northward volume transport to heat transport

The climatic relevance of the AMOC arises from its association with the northward heat transport. This aspect is assessed by correlating the annual-mean time series of AMOC to that of the ocean heat transport (AOHT) at different latitudes (Fig. 5) in the North Atlantic. This analysis can only be done for HadCM3, FAMOUS, FORTE, HiGEM and partly for CHIME. (AOHT is unavailable for other RAPID models and most of the CMIP3 models.) The time-mean heat transport is maximum around 10–30° N, where it is about 1 PW (Fig. 6a, Table 1) in models. Compared to the observational estimate of Ganachaud and Wunsch (2003), HiGEM and FORTE values are within the error bars of 2 of the 3 North Atlantic latitudes, while HadCM3 and CHIME are closer to the estimate around 50 N. FAMOUS heat transports are generally underestimated. Like T_{over}, AOHT does not have a well-defined maximum in variability as a function of latitude (Fig. 6b). Though the volume and heat transport variations in the models do not have a similar zonal profile, in general a good degree of temporal correlation is found between them at all latitudes from 15° N to 45° N (Figs. 5, 3b, Table 1 for 26° N). The slopes of the regression are fairly similar between 26–45° N, indicating the positive volume-heat transport relationship at these latitudes. However, since the AMOC at 26° N and 50° N are not strongly correlated (Sect. 5), we expect that AOHT at 50° N, in the latitudes of the Northern Europe, is not strongly correlated with the AMOC at 26° N. Indeed this is the case in HadCM3, FAMOUS, FORTE, CHIME and HiGEM (Table 1).

OSD
8, 1–28, 2011

7 Concluding remarks

We have shown that the 5-daily standard deviation of the AMOC simulated in the RAPID set of coupled climate models is comparable to that of the RAPID/MOCHA observational estimate from the array at about 26° N. This is an evaluation of a property that is unlikely to have been "tuned" during model development, because the observational estimate is new. Surprisingly, there is no systematic relation between the model resolution and the magnitude of variability. The standard deviation has contributions from high-frequency variability (timescale of a few days), the annual cycle and interannual variability. The models generally have more high-frequency variability than that estimated from observations, and a similar amplitude of annual cycle, but a spread in simulating the shape of the cycle. The observational dataset (of 5 years) as yet is not long enough to assess simulated interannual variability. In the RAPID models and in most CMIP3 AOGCMs, the magnitude of interannual variability in the AMOC at 26° N and in the maximum of the AMOC are similar, the latter being a commonly used model index.

We have dynamically decomposed the variability at about 29° N (slightly north of the RAPID/MOCHA array in order to avoid complications with model coastlines) into Ekman, geostrophic (i.e. due to pressure and sea-level gradient) and viscous/frictional components. The AMOC at 29° N is predominantly geostrophic, but the Ekman term also contributes to variability. Ekman variability is more important in models than in observations. Other ageostrophic terms contribute non-negligible variability in models, but are neglected in the observational estimate. Our study implies that such a decomposition of the transport is worth checking in the future intercomparison studies of AOGCMs in order to gain a better understanding of the processes responsible and the realism of their simulation.

Considering annual timeseries, we find that Atlantic Ocean heat transport is fairly well correlated with the AMOC at each latitude, as expected, confirming its climatic significance. Correlation between different latitudes is dominated by long-range

OSD
8, 1–28, 2011

geostrophic coherence. But it does not extend over the whole basin (also found by Lozier et al., 2010). Consequently the AMOC at 26° N does not have a high correlation with the AMOC or with heat transport at mid-to-high latitudes. Since the latter has a practical importance, and because this analysis, Zhang (2010) and Hodson and Sutton (2011) all suggest that AMOC variability on multiannual timescales propagates from north to south, it would be useful to monitor the AMOC at higher latitudes as well as at 26° N.

Acknowledgement. This study was supported by the "UK RAPID Thermohaline Circulation Coupled Model Intercomparison Project" (UKTHCMIP) of the RAPID programme of the Natural Environment Research Council, under grants NERC NE/C509366/1 and NE/C522268/1. Data from UKTHCMIP are available from the British Atmospheric Data Centre. Data from the RAPID-WATCH MOC monitoring project are funded by the NERC and are available from www.noc.soton.ac.uk/rapidmoc. We acknowledge the CMIP3 modelling groups for making their model output available as, the Program for Climate Model Diagnosis and Intercomparison (PCMDI) for collecting and archiving this data, and the WCRP's Working Group on Coupled Modelling (WGCM) for organizing the model data analysis activity. The WCRP CMIP3 multimodel dataset is supported by the Office of Science, US Department of Energy. Jonathan Gregory was partly supported by the Joint DECC and Defra Integrated Climate Programme, DECC/Defra (GA01101).

References

Baehr, J., Cunnningham, S., Haak, H., Heimbach, P., Kanzow, T., and Marotzke, J.: Observed and simulated estimates of the meridional overturning circulation at 26.5° N in the Atlantic, Ocean Sci., 5, 575–589, doi:10.5194/os-5-575-2009, 2009.

Biastoch, A., Böning, C. W., Getzlaff, J., Molines, J.-M., and Madec, G.: Mechanisms of interannual-decadal variability in the meridional overturning circulation of the mid-latitude North Atlantic Ocean, J. Climate, 21, 6599–6615, doi:10.1175/2008JCLI2404.1, 2008.

Bigg, G. R. and Wadley, M. R.: Millennial changes in the oceans: an ocean modeller's viewpoint, J. Quaternary Sci., 16, 309–319, 2001.

OSD

8, 1–28, 2011

Bingham, R. J., Hughes, C. W., Roussenov, V., and Williams, R. G.: Meridional coherence of the North Atlantic meridional overturning circulation, Geophys. Res. Lett., 34, L23606, doi:10.1029/2007GL031731, 2007.
Blaker, A. T., Sinha, B., Wallace, C., Smith, R., and Hirschi, J. J.-M.: A description of the FORTE 2.0 coupled climate model, Geosci. Model Dev., in preparation, 2011.
Bleck, R.: An oceanic general circulation model framed in hybrid isopycnic-cartesian coordinates, Ocean Model., 4, 55–88, 2002.
Collins, M., Botzet, M., Carril, A. F., Drange, H., Jouzeau, A., Latif, M., Masina, S., Otteraa, O. H., Pohlmann, H., Sorteberg, A., Sutton, R. T., and Terray, L.: Interannual to decadal climate predictability in the North Atlantic: a multimodel-ensemble study, J. Climate, 19, 1195–1202, 2006.
Cunningham, S. A., Kanzow, T., Rayner, D., Baringer, M. O., Johns, W. E., Marotzke, J., Longworth, H. R., Grant, E. M., Hirschi, J. J.-M., Beal, L. M., Meinen, C. S., and Bryden, H.: Temporal variability of the Atlantic meridional overturning circulation at 26.5°N, Science, 317, 935–938, 2007.
Dong, B.-W. and Sutton, R. T.: The dominant mechanisms of variability in Atlantic Ocean heat transport in a coupled ocean-atmosphere GCM, Geophy. Res. Lett., 28, 2445–2448, 2001.
Edwards, N. R. and Marsh, R.: Uncertainties due to transport-parameter sensitivity in an efficient 3-D ocean climate model, Clim. Dynam., 24, 415–433, 2005.
Ganachaud, A. and Wunsch, C.: Large scale ocean heat and freshwater transports during the World Ocean Circulation Experiment, J. Climate, 16, 696–705, 2003.
Gordon, C., Cooper, C., Senior, C. A., Banks, H., Gregory, J. M., Johns, T. C., Mitchell, J. F. B., and Wood, R. A.: The simulation of SST, sea ice extents and ocean heat transports in a version of the Hadley Centre coupled model without flux adjustments, Clim. Dynam., 16, 147–168, doi:10.1007/s003820050010, 2000.
Gregory, J. M., Dixon, K. W., Stouffer, R. J., Weaver, A. J., Driesschaert, E., Eby, M., Fichefet, T., Hasumi, H., Hu, A., Jungclaus, J. H., Kamenkovich, I. V., Levermann, A., Montoya, M., Murakami, S., Nawrath, S., Oka, A., Sokolov, A. P., and Thorpe, R. B.: A model intercomparison of changes in the Atlantic thermohaline circulation in response to increasing atmospheric CO_2 concentration, Geophys. Res. Lett., 32, L12703, doi:10.1029/2005GL023209, 2005.
Hodson, D. L. R. and Sutton, R. T.: The impact of model resolution on MOC adjustment in a coupled climate model, Clim. Dynam., in preparation, 2011.
Hirschi, J. J.-M., Baehr, J., Marotzke, J., Stark, J., Cunningham, S., and Beismann, J.-O.:

OSD
8, 1–28, 2011

A monitoring design for the Atlantic meridional overturning circulation, Geophy. Res. Lett., 30, 1413, doi:10.1029/2002GL016776, 2003.
Jones, C., Gregory, J. M., Thorpe, R., Cox, P., Murphy, J., Sexton, D., and Valdes, P.: Systematic optimisation and climate simulations of FAMOUS, a fast version of HadCM3, Clim. Dynam., 25, 189–204, 2005.
Keenlyside, N. S., Latif, M., Jungclaus, J., Kornblueh, L., and Roeckner, E.: Advancing decadal-scale climate prediction in the North Atlantic sector, Nature, 453, 84–88, 2008.
Knight J. R., Allan, R. J., Folland, C. K., Vellinga, M., and Mann, M. E.: A signature of persistent natural thermohaline circulation cycles in observed climate, Geophys. Res. Lett., 32, L20708, doi:10.1029/2005GL024233, 2005.
Lozier, M. S., Roussenov, V., Reed, M. S. C., and Williams, R. G.: Opposing decadal changes for the North Atlantic meridional overturning circulation, Nature Geosci., 3, 728–734, doi:10.1038/ngeo947, 2010.
Meehl, G. A., Stocker, T. F., Collins, W. D., Friedlingstein, P., Gaye, A. T., Gregory, J. M., Kitoh, A., Knutti, R., Murphy, J. M., Noda, A., Raper, S. C. B., Watterson, I. G., Weaver, A. J., and Zhao, Z.-C.: Global Climate Projections, Climate Change 2007: The Physical Science Basis, Contribution of Working Group I to the Fourth Assessment Report of the Intergovernmental Panel on Climate Change, edited by: Solomon, S., Qin, D., Manning, M., Chen, Z., Marquis, M., Averyt, K. B., Tignor, M., and Miller, H. L., Cambridge University Press, Cambridge, UK and New York, NY, USA, 2007.
Megann, A. P., New, A. L., Blaker, A. T., and Sinha, B.: The sensitivity of a coupled climate model to its ocean component, J. Climate, 23, 5126–5150, 2010.
Pacanowski, R. C.: MOM 1 Documentation Users Guide and Reference Manual GFDL Ocean Technical Report, Geophysical Fluid Dynamics Laboratory, NOAA, Princeton, USA, 1990.
Schmittner, A., Latif, M., and Schneider, B.: Model projections of the North Atlantic thermohaline circulation for the 21st century assessed by observations, Geophys. Res. Lett., 32, L23710, doi:10.1029/2005GL024368, 2005.
Shaffrey, L. C., Stevens, I., Norton, W. A., Roberts, M. J., Vidale, P. L., Harle, J. D., Jrrar, A., Stevens, D. P., Woodage, M. J., Demory, M. E., Donners, J., Clark, D. B., Clayton, A., Cole, J. W., Wilson, S. S., Connolley, W. M., Davies, T. M., Iwi, A. M., Johns, T. C., King, J. C., New, A. L., Slingo, J. M., Slingo, A., Steenman-Clark, L., and Martin, G. M.: UK-HiGEM: The new UK High Resolution Global Environment Model. Model description and basic evaluation, J. Climate, 22, 1861–1896, 2009.

OSD
8, 1–28, 2011

Smith, R., Osprey, A., and Gregory, J. M.: A description of the FAMOUS (version XDBUA) climate model and control run, Geosci. Model Dev., 1, 53–68, 2008.

Stouffer, R. J., Yin, J., Gregory, J. M., Dixon, K. W., Spelman, M. J., Hurlin, W., Weaver, A. J., Eby, M., Flato, G. M., Hasumi, H., Hu, A., Jungclaus, J. H., Kamenkovich, I. V., Levermann, A., Montoya, M., Murakami, S., Nawrath, S., Oka, A., Peltier, W. R., Robitaille, D. Y., Sokolov, A., Vettoretti, G., and Webber, S. L.: Investigating the causes of the response of the thermohaline circulation to past and future climate changes, J. Climate, 19, 1365–1387, 2006.

Vellinga, M. and Wood, R. A.: Global climatic impacts of a collapse of the Atlantic thermohaline circulation, Clim. Change, 54, 251–267, 2002.

Weaver, A. J., Eby, M., Wiebe, E. C., Bitz, C. M., Duffy, P. B., Ewen, T. L., Fanning, A. F., Holland, M. M., MacFadyen, A., Matthews, H. D., Meissner, K. J., Saenko, O., Schmittner, A., Wang, H., and Yoshimori, M.: The UVic Earth System Climate Model: model description, climatology and application to past, present and future climates, Atmos.-Ocean, 39, 361–428, 2001.

Webb, D. J.: An ocean model code for array processor computers, Comput. Geosci., 22, 569–578, 1996.

Webb, D. J., de Cuevas, B. A., and Richmond, C. S.: Improved advection schemes for ocean models, J. Atmos. Ocean. Technol., 15, 1171–1187, 1998.

Zhang, R.: Latitudinal dependence of Atlantic meridional overturning circulation (AMOC) variations, Geophys. Res. Lett., 37, L16703, doi:10.1029/2010GL044474, 2010.

OSD

8, 1–28, 2011

Table 1. Specifications of the RAPID-models; time-mean and standard deviations ($X(Y)$ indicates X is mean and Y is SD) of simulated Atlantic ocean meridional overturning transport (in Sv), T_{over}, at 26° N and of the maximum of Atlantic MOC, M_{max} on 5-daily and annual timescales; time-mean and standard deviation (SD) of the simulated 5-daily T_{over}, 29° N and its decomposed components (T_{Ek}: Ekman part, T_{geo}: geostrophic part, T_{vis}: viscous/frictional part and T_{adv}: advection part); time-mean of simulated annual ocean meridional heat transport (AOHT in PW), 26° N and the interannual correlation T_{over} at 26° N with M_{max}, AOHT at 26° N and AOHT at 50° N. The RAPID/MOCHA observational estimate (of 5 years) is given in the last column. In HiGEM and FORTE, the transport component due to viscous part has 2 parts namely, by the laplacian and biharmonic terms. In FORTE, the biharmonic term is implicit and could not be calculated offline. The FRUGAL transport at 26° N is calculated along a curvilinear gridline which is near 26° N. Time-step data is used in GENIE which has an ocean time-step of 3.65 days. GENIE has no seasonal variability in wind-stress and no interannual variability. Meridional correlation length (in °lat) at 26° N is defined as the latitudinal extent of positive correlation above 0.5 in both directions. FRUGAL and CHIME data are only available for some of the calculations.

Model	HadCM3	FAMOUS	FRUGAL	FORTE	GENIE	CHIME	HiGEM	OBS
Atmos res: lon × lat × level	3.75 × 2.5 × 19	HadCM3 at 7.5 × 3.75 × 11	Enhanced UVic	IGCM3 T42 × 15	UVic 2-D	HadCM3 atmos	HadGEMI at 1.25 × 0.83 × 38	
Ocean res: lon × lat × level	1.25 × 1.25 × 20	HadCM3 at 3.75 × 2.5 × 20	MOM V2 with high-res Arctic	MOM 2 × 2 × 15	GOLDSTEIN 10 × 5 × 8	HYCOM at 1.25 × 1.25 × 25	HadGEMI at 0.33 × 0.33 × 40	
T_{over} (Sv)								
Latitude° N/Depth (m)	26.3/995	26.3/995		26.0/1365	26.4/1158	26.3/1050	26.9/959	26.5/1041
5-daily, 1 yr	19.2 (4.2)	18.9 (4.2)	26.4 (1.3)	16.3 (4.2)	16.4 (0.3)	15.2 (3.8)	15.1 (2.7)	20.5 (4.1)
5-daily, 10 yr	17.1 (4.1)	18.2 (4.2)	26.4 (1.4)	17.2 (4.5)	16.4 (0.3)	15.0 (3.3)	15.5 (4.0)	18.6 (4.5)
Annual	16.8 (0.9)	20.6 (1.3)		17.6 (1.1)	16.5 (0)	18.8 (1.2)	16.4 (1.0)	
M_{max} (Sv)								
5 d–10 yrs	21.9 (2.4)	18.7 (3.0)	26.5 (1.3)	21.3 (2.5)	18.5 (0.3)		20.6 (2.5)	
Annual	18.9 (0.7)	20.0 (1.3)		19.8 (1.1)	18.6 (0)	20.1 (1.7)	18.9 (1.1)	
Dynamical decomposition of T_{over} (Sv) for 5-daily means (except time-step for GENIE)								
Latitude° N/Depth(m)	28.8/995	28.8/995		30/1365	30/1158		28.9/959	26.5/1041
Overturning T_{over}	18.0 (4.3)	18.1 (3.7)		16.5 (3.9)	16.1 (0.12)		15.7 (3.6)	18.6 (4.5)
Ekman T_{Ek}	0.9 (4.0)	3.5 (3.5)		1.4 (3.8)	−2.3 (0)		1.6 (3.3)	3.6 (3.2)
Geostrophic T_{geo}	17.6 (2.3)	15.3 (1.6)		15.2 (2.8)	16.8 (0.1)		14.4 (2.6)	15.0 (3.5)
Viscous T_{vis}	−0.4 (0.1)	−0.8 (0.2)		−0.1(0.1)	1.7 (0.02)		−0.2 (0.0), −0.1 (0.1)	
Advective T_{adv}							0.3 (0.6)	
Correlation (T_{int}, T_{ext})	−0.98	−0.94		−0.64			−0.96	−0.83
Latitudinal variation of annual volume and heat transport								
Corr. length (°lat), 26° N	40	24		25			28	
Latitude of M_{max} (° N)	35–45	31–34		30–40	46–51	23–60	34–45	
Corr (T_{over} 26° N, M_{max})	0.38	0.96		0.70	0.93	0.53	0.74	
Mean AOHT, 26° N(PW)	1.0	0.8		1.1			1.1	
Corr (T_{over}, AOHT), 26° N	0.8	0.8		0.9			0.9	
Corr (T_{over} 26° N, AOHT50° N)	0.00	0.24		0.39		0.42	0.36	

OSD
8, 1–28, 2011

Table 2. Comparison of standard deviations (in Sv) of Atlantic MOC (T_{over}) at 26° N, 50° N and of the maximum of Atlantic MOC, M_{max}, and their correlations in the CMIP3 models. Linear or quadratic trend is removed for unsteady runs before the calculation. The lag between T_{over} at 26° N and 50° N is shown which gives the largest correlation of their timeseries. The lag is negative when T_{over} 26° N lags.

Model	SD M_{max}	SD T_{over} 26° N	Corr (T_{over} 26° N, M_{max})	SD T_{over} 50° N	Corr (T_{over} 26° N, T_{over}50° N)	Lag (years)	Lagged corr. (T_{over} 26° N, T_{over}50° N)
CSIRO-Mk3.0	1.8	1.6	0.85	1.6	0.53	−1	0.70
CNRM-CM3	1.8	2.1	0.20	1.7	0.05	−2	0.41
CCCMA-CGCM3.1(T63)	0.72	0.71	0.85	0.67	0.11	−1	0.51
CCCMA-CGCM3.1(T47)	0.50	0.63	0.09	0.65	−0.14	−2	0.39
BCCR-BCM2-0	0.93	0.91	0.61	0.82	−0.02	−2	0.25
GISS-ER	2.7	0.97	0.06	2	0.35	−1	0.48
GISS-AOM	7.2	1.5	0.01	2.0	0.19	−3	0.44
GFDL-CM2.1	1.3	1.2	0.39	1.1	−0.01	−5	0.46
GFDL-CM2.0	1.1	1.1	0.38	1.1	0.12	−2	0.51
CSIRO-Mk3.5	1.2	1.0	0.88	1.4	0.52	−1	0.72
MIROC3.2 (hires)	0.8	1.0	0.16	0.82	0.02	−1	0.28
INM-CM3.0	2.9	3.4	0.47	1.7	0.07	−2	0.52
INGV-ECHAM4	1.6	1.9	0.61	1.5	0.09	−3	0.58
IAP-FGOALS1.0g	2.3	0.49	0.09	0.43	−0.26	10	−0.02
NCAR-CCSM3.0	1.8	1.2	0.88	1.1	0.24	−2	0.45
MRI-CGCM2.3.2a	0.71	0.73	0.53	0.97	−0.23	−1	0.34
MIUB-ECHOG	1.3	1.0	0.35	1.2	0.23	−4	0.53
MIROC3.2 (medres)	0.72	0.64	0.67	0.69	0.07	−2	0.44
UKMO-HadGEM1	1.0	1.0	0.68	0.77	0.05	−1	0.21
UKMO-HadCM3	1.7	1.8	0.54	1.2	0.05	1	0.21

OSD
8, 1–28, 2011

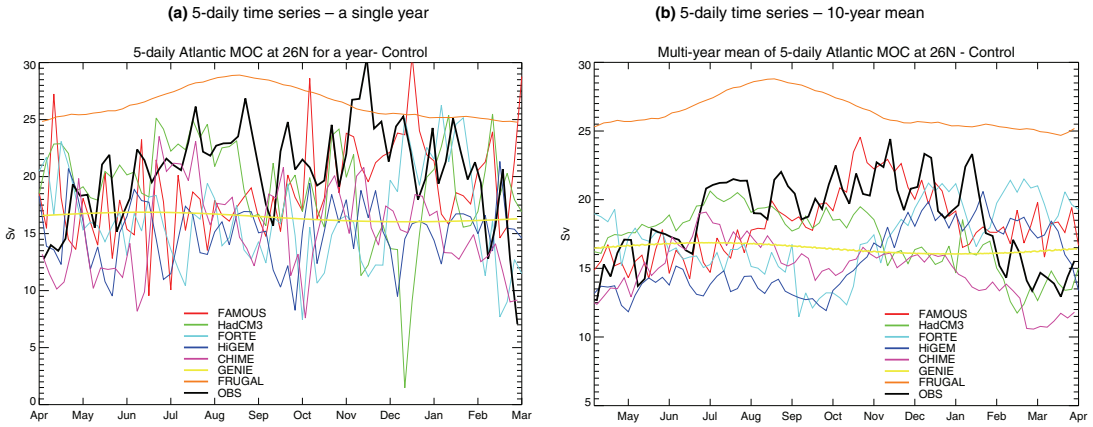

Fig. 1. Atlantic MOC (T_{over}) at 26° N **(a)** 5-daily time series – for a single year **(b)** 5-daily time series – 10-year mean in models and 5-year mean in observations (The FRUGAL transport is calculated along a curvilinear gridline which is near 26° N. For GENIE, time-step data is plotted; its ocean time-step is 3.65 days) **(c)** 5-daily – power spectrum (note the logarithmic scale on the *y*-axis. Oscillations of less than 40-day period are significant in observations and in all the models, except FRUGAL and GENIE), and **(d)** annual time series (HiGEM data is only 90 years long after the spin-up time).

OSD
8, 1–28, 2011

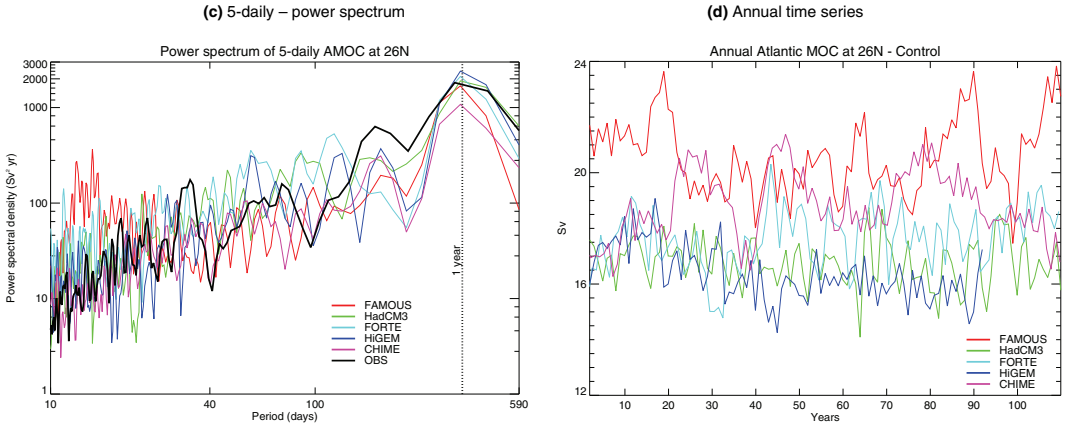

Fig. 1. Continued.

OSD
8, 1–28, 2011

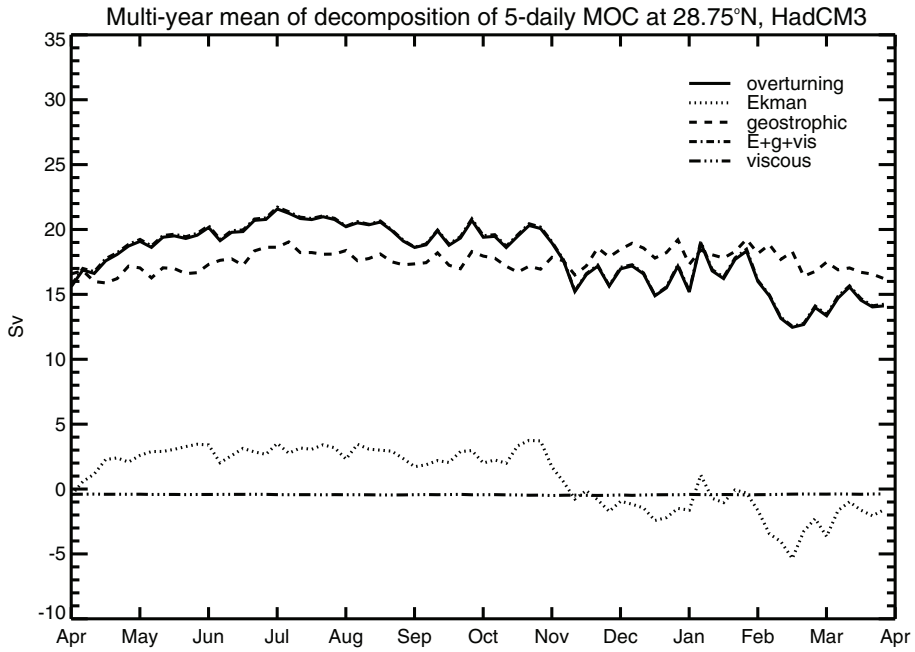

Fig. 2. Decomposition of 5-daily Atlantic MOC (T_{over}) into physical components at about 29° N in HadCM3. The sum E+g+vis (dash-dotted) is almost coincident with the total overturning (solid).

OSD
8, 1–28, 2011

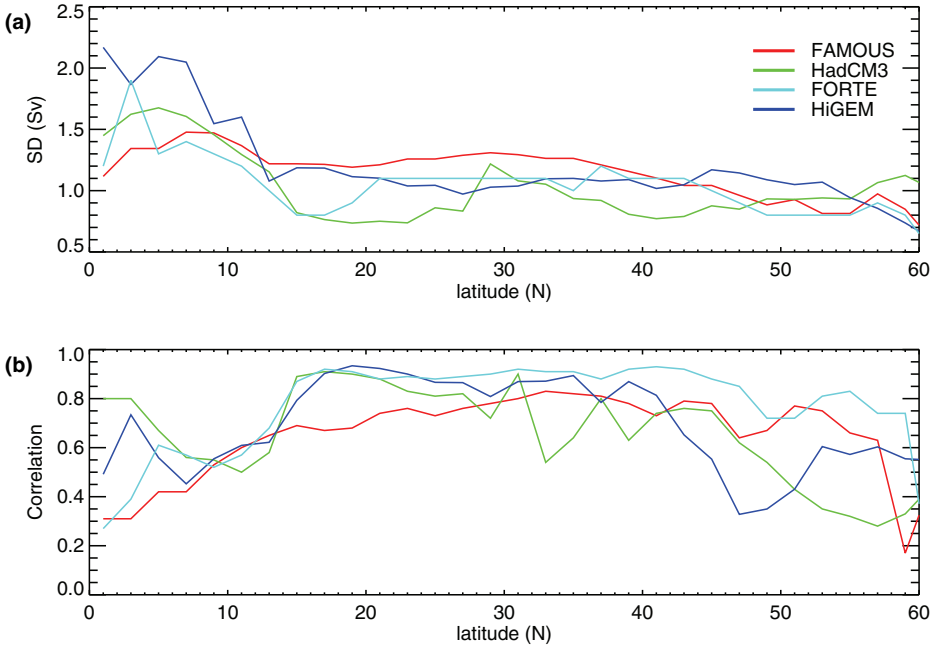

Fig. 3. Zonal profile of **(a)** annual ocean meridional overturning transport (T_{over}) variability (Sv) and **(b)** correlation of annual T_{over} and ocean meridional heat transport in the North Atlantic.

OSD
8, 1–28, 2011

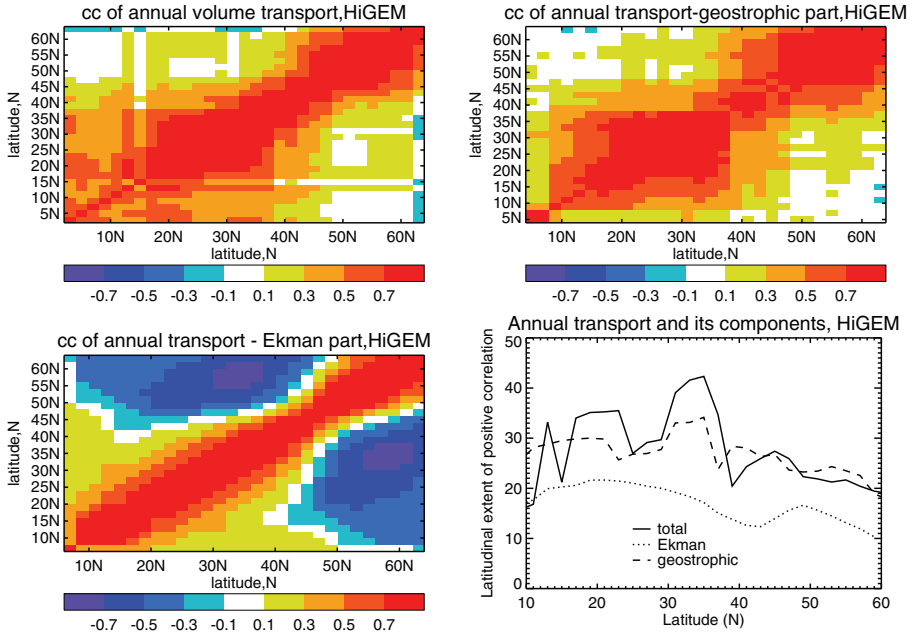

Fig. 4. Cross-correlation of annual ocean meridional overturning transport, T_{over} (top left) and its physical components – geostrophic, T_{geo} (top right), Ekman, T_{ek} (bottom left) between latitudes in the North Atlantic in HiGEM and their meridional correlation length (bottom right). Correlation length (°lat) as a function of latitude y is defined as the width of the range of latitudes whose timeseries which have a temporal correlation exceeding 0.5 with the timeseries at latitude y.

OSD
8, 1–28, 2011

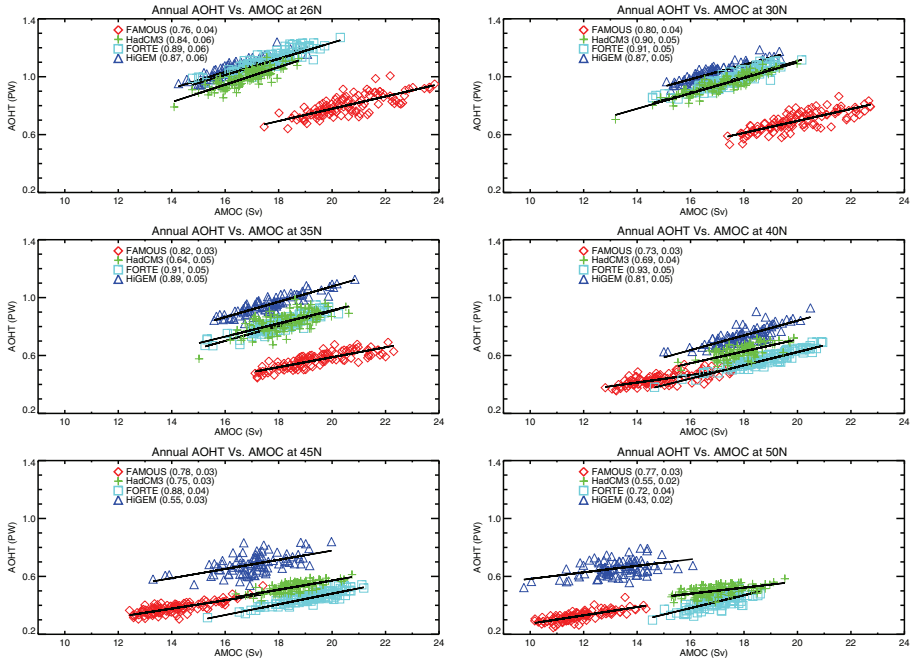

Fig. 5. Scatter plot of annual-mean ocean meridional overturning transport, T_{over} (Sv) and ocean meridional heat transport (PW) at various latitudes in the North Atlantic in different models. The correlation coefficients and slopes of the regression are given in brackets.

OSD
8, 1–28, 2011

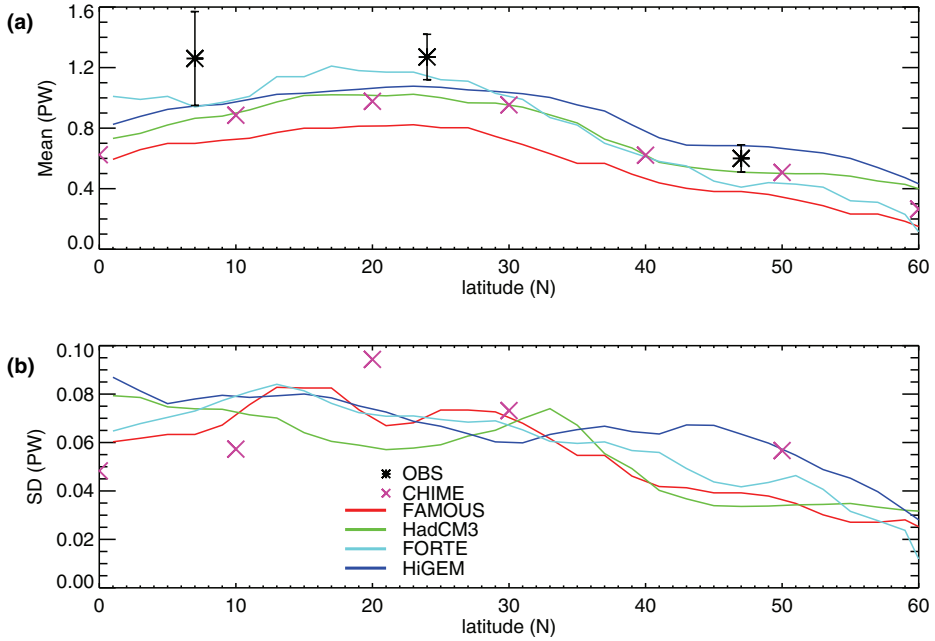

Fig. 6. Zonal profile of **(a)** mean annual ocean meridional heat transport (PW) and **(b)** variability of annual ocean meridional heat transport in the North Atlantic. The observational estimate of heat transport is from Ganachaud and Wunsch (2003). CHIME data is only available in 10° latitude intervals.

OSD
8, 1–28, 2011